ACS APPLIED MATERIALS & INTERFACES

Research Article

www.acsami.org

Highly Luminescent and Nontoxic Amine-Capped Nanoparticles from Porous Silicon: Synthesis and Their Use in Biomedical Imaging

Jayshree H. Ahire,[†] Qi Wang,[†] Paul R. Coxon,[†] Girish Malhotra,[‡] Rik Brydson,[§] Rongjun Chen,[‡] and Yimin Chao*,[†]

[†]Energy Materials Laboratory, School of Chemistry, University of East Anglia, Norwich NR4 7TJ, United Kingdom

[‡]Centre for Molecular Nanoscience, School of Chemistry, and [§]Institute for Materials Research, SPEME, University of Leeds, Leeds LS2 9JT, United Kingdom

Supporting Information

ABSTRACT: Stable and brightly luminescent amine-terminated Si nanoparticles (SiNPs) have been synthesized from electrochemically etched porous silicon (PSi). The surface amine termination was confirmed by FTIR, NMR, and XPS studies. The mean diameter of the crystal core of 4.6 nm was measured by transmission electron microscopy (TEM), which is in a good agreement with the size obtained by dynamic light scattering (DLS). The dry, amine-terminated product can be obtained from bulk silicon wafers in less than 4 h. This represents a significant improvement over similar routines using PSi where times of >10 h are common. The emission quantum yield was found to be about 22% and the nanoparticles exhibited an exceptional stability over a wide pH range (4−14). They are resistant to aging over several weeks. The amine-terminated SiNPs showed no significant cytotoxic effects toward HepG2 cells, as assessed with MTT assays.

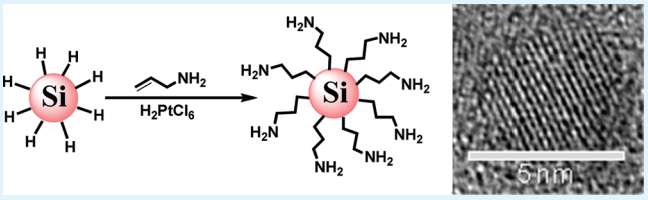

KEYWORDS: *cellular imaging, semiconductor nanoparticles, surface capping, photoelectron spectroscopy, FTIR, NMR*

1. INTRODUCTION

Over the last 20 years, silicon nanoparticles (SiNPs), or "quantum dots" (QDs), have attracted tremendous interest from the scientific community because of their unique characteristics that differ from those of their bulk counterparts, such as novel optical, catalytic, electronic, and mechanical properties.[1,2] At nanometer scales, silicon exhibits visible photoluminescence (PL) because of the quantum confinement effect that can be exploited for uses in electronic and photonic devices.[3,4] Indeed, silicon has several advantages to be an ideal nanoparticle material such as size-dependent tunable light emission,[5−7] high brightness,[8] and their great stability against photobleaching compared to organic dye molecules.[9,10] These properties have helped establish silicon-based nanoparticles in a whole swathe of diagnostic and assay roles as fluorescent cellular markers.[11,12] Furthermore, silicon exhibits a low inherent toxicity in comparison with the heavy elements of several other types of semiconductor quantum dots which can pose significant risks to human health.[12−15] The combination of these properties opens a new avenue of applications of SiNPs for optoelectronic and bioimaging purposes.[16−18]

Silicon is an indirect bandgap material and shows remarkable changes in its optical properties when the particle diameter is reduced to less than the bulk Bohr exciton radius (4.6 nm for silicon).[19,20] Silicon nanoparticles can be synthesized by a wide range of chemical or physical methods, including solution routes using a variety of reducing agents,[21,22] the microemulsion technique,[20,23] ultrasonic dispersion of electrochemically etched silicon,[3,24,25] laser-induced pyrolysis of silane,[26,27] synthesis in inverse micelles.[10] Chemical routes tend to have higher product yields, though often at the expense of particle homogeneity and tight size control, while physical routes generally produce small quantities mainly for physical or electronic applications. Nanoparticles produced by chemical routes may also be compatible with the conjugation of biological molecules at the particle surface.[28]

For silicon quantum dots to be employed within biomedical applications, it is essential that they are water-soluble and hydrophilic to prevent aggregation and precipitation in a biological environment, have a substantial photoluminescence quantum yield in the visible region and a fast radiative recombination rate. The chemical process used to terminate the surfaces of the silicon QDs changes the internal electronic structure and thus plays an important role in the resultant emission wavelength and radiative lifetime, and ultimately determines the solubility.[29] The visible luminescence from Si nanocrystals has been attributed to the decay of quantum-confined excitons,[30] as well as decay mechanisms mediated by surface atoms.[31] The exciton can occur via an energy level located in the band gap,[32] or via energy transfer to a covalently attached dye with a suitable excitation energy.[33] Quantum confinement and thus the PL emission is controlled by the size

Received: April 12, 2012
Accepted: May 24, 2012
Published: May 24, 2012

of the core of the NPs, but because of the high surface to volume ratio, the chemistry at the NPs' surface also plays a crucial role.

Here we have demonstrated a simple room-temperature synthesis of amine-terminated silicon nanoparticles, which are soluble in water and exhibit strong blue photoluminescence at room temperature. Here, the nanoparticles are derived from hydrogen-terminated SiNPs, a common starting material for that is ideally suited to further functionalization, cleaved from the porous layer of an electrochemically etched silicon wafer in hydrofluoric acid (HF) and ethanol in a simple and short reaction step. This is a key difference from other reported routines of aminoalkyl-terminated SiNPs which typically involve an intermediate step via bromination before the final capping layer is formed and reaction times of upward of at least 10 h.[34−36] Here, a dried powder of nanoparticles can be obtained in under 4 h, at room temperature, and uses a simple metallic catalyst which is easily removed and ensures a highly pure final product. The advantages of using porous silicon as a starting material lie in the relative simplicity of its preparation, the high product yields gained, and excluding the necessary etching fluids, is a relatively environmentally friendly process. The latter point is of particular concern as the applications of nanomaterials continue to expand and more people come into contact with them. Nanoparticles are widely anticipated to find uses in a growing number of commercial and clinical products and devices,[37] and so health and environmental impact of the synthesis and handling procedures used is likely to come under increasing scrutiny.

2. EXPERIMENTAL SECTION

2.1. Synthesis of Amine-Capped SiNPs. A hydrogen-terminated porous silicon layer was formed by galvanostatic anodization of a boron-doped *p*-Si (100) chip (size approximately 1.25 cm × 1.25 cm, 10 Ω cm^{-1} resistivity, Compart Technology, Peterborough, U.K.) in a 1:1 v/v solution of 48% aqueous HF and ethanol using our modified

Scheme 1. Synthesis of Hydrogen-Terminated Silicon Nanoparticles Using Porous Silicon

$$Si + 6HF \xrightarrow{EtOH} H_2SiF_6 + H_2 + np\text{-}Si\text{-}H + 2H^+ + 2e^-$$

method as described by Chao et al.,[3] see Scheme 1. The electrochemical cell was machined from PTFE and circular in cross-section (1 cm diameter). The silicon wafer was sealed to the base using a Viton O-ring. The etching was carried out using a constant current source (Keithley SourceMeter 2601). A layer of luminescent porous silicon was made at high current density (at 400 mA cm^{-2} for 5 min). The reacted solution was decanted, and the hydrogen-terminated porous silicon chips were dried under vacuum for 2 h. Amine-terminated nanoparticles were obtained by reacting the hydrogen-terminated porous silicon with allylamine (0.5 mL) within a Schlenk flask under N_2, in the presence of 0.05 M H_2PtCl_6 (40 μL) catalyst in isopropanol. After 30 min of sonication, the resulting reaction mixture was filtered and dried. The resulting amine-terminated SiNPs were washed three times with dichloromethane in order to remove the impurities and dried under vacuum, see Figure S8 in the Supporting Information. A solid brown powder of the amine-terminated SiNP product was obtained, see Scheme 2. Thirty milligrams of dry powder was obtained from each reaction. This powder was redissolved in water for further characterization. After ultrasonic induced attachment of amine onto the silicon nanoparticle, the surface dispersed grafted particles become soluble, highly stable in water and show blue-green visible photoluminescence when exposed to ultraviolet light.

Scheme 2. Functionalization of Hydrogen-Terminated Silicon Nanoparticles Using Allylamine and Catalytic Amount of Pt Catalyst

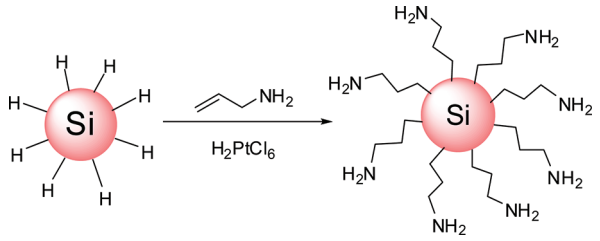

2.2. Size Measurement with TEM and DLS. Transmission electron microscopy (TEM) studies were performed with a JEOL (JEM- 2000 Ex) microscope and high-resolution TEM was performed with a Philips CM200 FEGTEM microscope. TEM samples were prepared by dipping a carbon-coated 300 mesh copper grid into a filtered solution of SiNPs in water. The solvent was evaporated and TEM micrographs were typically taken at different spots of each grid.

Dynamic light scattering (DLS) measurements were recorded using the Zetasizer Nano ZS (Malvern Instruments Ltd., UK). Samples from pure amine-terminated silicon nanoparticles were dissolved in water and the effective diameters were measured at room temperature.

2.3. Surface Chemical Bonding Information by FTIR, NMR, and XPS. FTIR measurements (Perkin-Elmer FTIR spectrometer) were carried out using a liquid cell that is made up of calcium chloride. The sample was dissolved in chloroform and injected into the liquid cell, and the measurements were then carried out by correcting the background.

^1H NMR (400 MHz) spectra of samples in D_2O and $CDCl_3$ were recorded on a Varian Unity Inova 400 MHz spectrometer. The fresh sample was dried under vacuum and redissolved in D_2O and $CDCl_3$, respectively.

X-ray photoelectron spectroscopy (XPS) measurements were performed with a SCIENTA ESCA300 XPS analyzer at the National Centre for Electron Spectroscopy and Surface Analysis (NCESS), Daresbury Laboratory, U.K.. A few drops of the suspension of SiNPs in dichloromethane were cast onto a freshly cleaned gold substrate. The sample was introduced immediately into a nitrogen-filled load-lock and allowed to dry before being transferred into the instrument chamber where the base pressure was kept below 1×10^{-8} mbar. All spectra were acquired at room temperature in normal emission, and the energy resolution was kept under 0.4 eV. In all photoemission spectra, binding energies (BEs) were referenced to the $Au4f_{7/2}$ line measured on a gold foil in direct electrical contact with the sample, which was found at a BE of 83 eV.

2.4. Absorption and Luminescence Spectroscopy. Absorption spectra were recorded in a quartz cuvette (10 × 10 mm), using a PerkinElmer 35 UV−vis double-beam spectrophotometer. The recorded spectra were scanned over a 300−700 nm range at a rate of 900 nm per min and corrected by subtracting the background contribution from the dispersing solvent.

The PL spectra were collected with a PerkinElmer LS55 spectrophotometer with an excitation slit width of 10 nm and an emission slit width set at 5 nm. The excitation wavelength was fixed at 360 nm. The emission spectra were corrected using the solvent emission as background.

The quantum yield of the amine-capped SiNPs was calculated with eq 1

$$Q = Q_R\left(\frac{\text{grad}}{\text{grad}_R}\right)\left(\frac{\eta^2}{\eta_R{}^2}\right) \quad (1)$$

Where Q is the quantum yield, grad is the gradient from a plot of integrated fluorescence intensity against absorbance. The subscript R refers to the reference fluorophore of known quantum yield. Here Quinine Sulfate was used as reference, which has a quantum yield of 54.6% when dissolved in 1N H_2SO_4. 1N (0.5M) H_2SO_4 had a

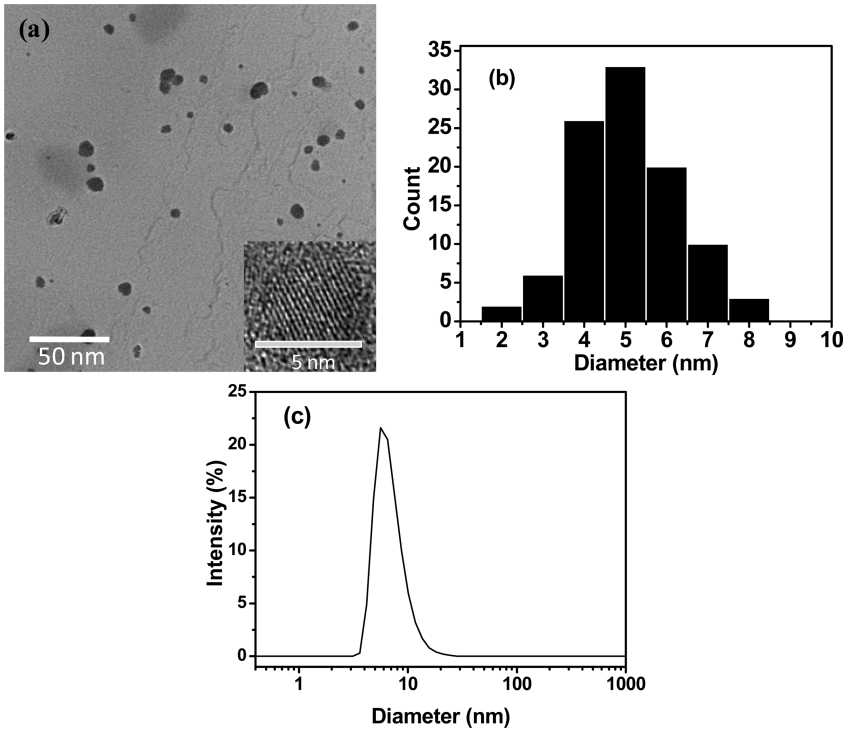

Figure 1. (a) TEM image of amine-terminated SiNPs and inset showing a high-resolution TEM image of an individual silicon nanocrystal screening the crystal lattice planes. (b) Histogram showing size distribution of amine-terminated SiNPs. (c) Dynamic light scattering spectrum displays the size and distribution of amine-capped silicon nanoparticles in water.

refractive index η_R of 1.346, whereas the refractive index η of water was 1.33.

Different pH buffer solutions were prepared using pH 4 tablets and values were adjusted using 1 M NaOH solutions. For PL measurements at various pH values, the SiNPs were immersed in each pH solution for 2 days prior to measurement.

2.5. MTT Assay and Luminescence Staining of HepG2 Cells. To evaluate the cytotoxicity of synthesized nanoparticles, we performed an MTT [3-(4,5-dimethylthiazol-2-yl)-2,5-diphenyltetrazolium bromide] assay to determine cell proliferation.[38−42] MTT measures mitochondrial activity within cells using tetrazolium salts as mitochondrial dehydrogenase enzymes cleave the tetrazolium ring, which occurs only in living cells.[43] Briefly, HepG2 (human liver hepatocellular carcinoma) cells were seeded in a 96-well plate for 24 h. Then the cells were treated with amine-capped SiNPs at various concentrations (0, 1, 5, 10, 50, 100, and 200 μg mL^{-1}) for a period of 48 h. All experiments were repeated at least three times. After incubation the medium was removed and followed by washing the cells with phosphate buffered saline (PBS). Then, the medium was changed and incubated with the MTT solution (5 mg mL^{-1}) for 2 h. The medium was removed, and formazan was solubilized in dimethylsulfoxide (DMSO). The absorbance was recorded on a microplate reader at the wavelength of 540 nm. The percentage of viable cells was estimated by direct comparison against the untreated control cells.

To prepare slides for confocal microscope imaging, HepG2 cells were seeded in a 35 mm Petri dish containing one slide each (density 1 × 10^6) in day 1. Amine-capped SiNPs (100 μg mL^{-1}) were added in day 3 (cells reach 50% confluence). The slides were incubated for 24 h at 37 °C inside a humidified incubator with a 5% CO_2 environment. The cells were washed twice with PBS, fixed with ice cold methanol for 5 min, then washed with PBS again. After this, they were stained with 1 mL of DAPI solution (20 μL stock diluted in 50 mL of PBS), incubated at room temperature for 30 min in the dark. Three microliters of mounting medium was used, and the slides were then coated with a solvent-based sealant. The slides were stored in a dark environment at −4 °C before images were taken.

3. RESULTS AND DISCUSSION

To determine the size and size distribution of the synthesized SiNPs, high-resolution TEM and DLS measurements were undertaken. The solid powder of pure amine-terminated SiNPs was dissolved in water and further measurement was conveyed. Figure 1a shows a TEM image of a number of amine-capped SiNPs on a carbon-coated copper grid.

Figure 1b shows histogram size distribution of amine-terminated SiNPs. A mean size and size distribution of 4.6 ± 1.9 nm was obtained by analyzing 100 nanoparticles from different regions of the grid, which is close to the exciton Bohr radius of silicon 4.3 nm. The inset in Figure 1a shows the highly crystalline structure of the atomic lattices. The lattice spacing of 0.31 nm is consistent with the Si (111) plane. DLS spectra confirm that the mean size of the amine terminated silicon NPs is 7.5 ± 1.0 nm, see Figure 1c. This mean size obtained from DLS is slightly larger than the one gained from TEM measurements, because the amine groups render SiNPs hydrophilicity and form a hydration shell.[44] Additional HRTEM images are shown in Figure S1 in the Supporting Information.

To confirm that the surface of silicon nanoparticle is completely covered with Si−C bonded amine moiety, we took FTIR spectra in normal transmission alignment. The spectrum was obtained from fresh sample dissolved in chloroform (Figure 2). From the FTIR spectrum, the observed bands at 1457 and 1260 cm^{-1} are attributed to Si-CH_2 vibrational scissoring and symmetric bending.[45] The features observed around 2853 to 2926 cm^{-1} are attributed to the C−H stretching of alkane. The transmittance between 3500 to 3690 cm^{-1} is assigned to the N−H stretching of an amine.[46] The band at 1605 cm^{-1} is attributed to allylamine N−H scissoring. The features between 920 and 1110 cm^{-1} are attributed to the

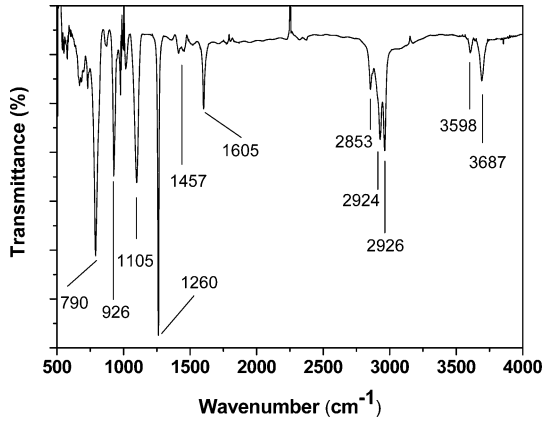

Figure 2. FTIR spectrum of amine-capped SiNPs in chloroform (32 scans, 4 cm^{-1} resolution).

vibrational stretching of Si-OR molecular components. The band at 790 cm^{-1} is N−H wagging. These features highlight the strength and stability of the Si−C bond formed between the silicon nanoparticles and the allylamine as well as the minimal number of Si-OR surface bonds present.[10] Similar features can be found in solid-phase FTIR shown in Figure S9 in the Supporting Information.

The surface chemistry of SiNPs was further confirmed by NMR. Figure 3 shows the NMR spectra of amine capped silicon nanoparticles in D_2O. A doublet of triplet (dt) peak is found between 3.38 and 3.42 ppm which is attributed to the protons adjacent to amine group.[46] The protons of the amine group were also observed at 1.18 ppm in $CDCl_3$ NMR (see Figure S10 in the Supporting Information). The sharp singlet at 4.6 ppm is arisen from the dispersing solvent.

Furthermore, the surface chemical bonding was studied using high resolution XPS spectroscopy. Figure 4 shows high-resolution XPS spectra of Si2p, C1s, O1s, and N1s region of a thin film of amine-terminated SiNPs. A full survey of the photoelectron spectrum is shown in the Supporting Information, Figure S11. The Si2p spectrum present in the Figure 4a is fitted with three peaks and a Shirley background. The three peaks are at 101.75, 102.80, and 100.74 eV. The first component is attributed to Si−C indicating that the surface of the SiNP is terminated with amine by replacing the hydrogen with amine. The second component is assigned to Si−O, which is indicative of the sample surface oxidation under ambient conditions. The third peak at 100.74 eV is attributed to Si−Si within silicon core of the SiNPs.[47,48] The C1s spectrum present in the Figure 4b is fitted with three components and a Shirley background. The three peaks are at 285.13, 286.45, and 284.45 eV, respectively. The first C1s peak at binding energy 285.13 eV is assigned to C−C or C−H bonding.[49,50] The second broad peak at 286.45 eV is ascribed to C−N bonding,[51] and third distinct peak at binding energy 284.45 eV is attributed to the C−Si bonding.[47] The existence of a C−Si component implies that the surface of the silicon nanoparticle changed from hydrogen to amine termination.

The O1s spectrum presented in the Figure 4c is fitted with two components and a Shirley background. The two components are at binding energy 532.68 and 534.23 eV respectively. The first distinct O1*s* peak at 532.68 eV is from Si−O group of the oxidized surface of SiNPs. The second component is possibly from hydroxide O−H group.[47] The N1*s* spectrum presented in Figure 4d is fitted with a single Gaussian and a Shirley background. The broad distinct peak is at 399.03 eV is attributed to the C−N bonding of the amine-terminated SiNPs.[51]

All data presented are from amine-capped SiNPs, because "uncapped" SiNPs as such do not exist. Without any capping, bare silicon nanoparticles are very quickly oxidized under ambient conditions and are not biocompatible. The propensity of nanoscale structures derived from bulk silicon through electrochemical etching to undergo surface oxidation in ambient conditions is a well-known effect that has been studied with both theoretical and experimental approaches.[52−54] Given the small size of nanoparticles studied here, once they are fully oxidized, they may no longer be described as silicon nanoparticles, and should properly be described as silica NPs. For the silicon nanoparticles described here, the initial hydrogen termination layer on the etched wafer serves a dual role: first as a convenient molecular anchor point at which surface modification may be performed and second as an interim guard against oxidation in order to preserve the chemical character of the silicon core prior to subsequent functionalization steps.

The absorption and emission spectra of amine-terminated SiNPs in water are presented in Figure 5a. The inset shows a photograph of the amine-capped SiNPs in water under UV illumination at 254 nm. The gradual increase in the absorbance with decreasing excitation wavelength from the onset wavelength of 450 nm, corresponding to the absorption edge of 2.75 eV, is characteristic of absorption across the indirect band gap of silicon.[55] The solid line shows the photoluminescence spectrum of amine capped SiNP in water at room temperature with the maximum emission peak centered at approximately 450 nm with a full width at half-maximum height of 107 nm under an excitation wavelength of 360 nm.

Photoluminescence quantum yields, see Figure 5b and Figures S2−S5 in the Supporting Information, of the amine-capped silicon nanoparticles in water were obtained using quinine sulfate (QY = 54.6%) as a reference emitter.[56] A

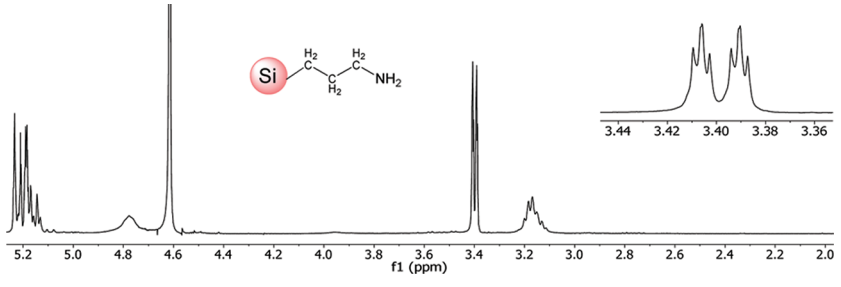

Figure 3. ^1H NMR spectrum amine-capped silicon nanoparticles in D_2O.

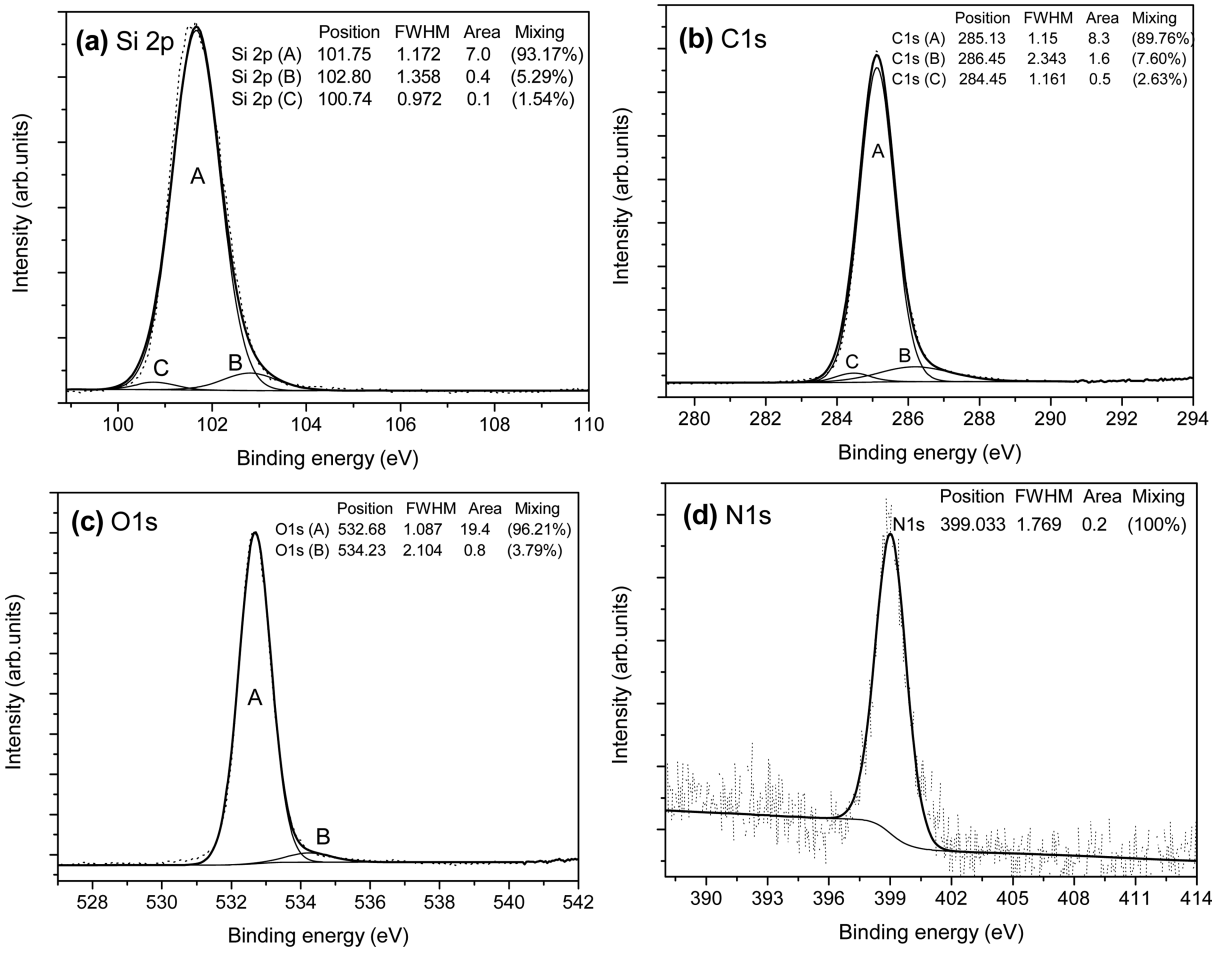

Figure 4. XPS core-level spectra of SiNPs obtained in normal emission with a photon energy 1486.6 eV: dotted line is experimental data that is fitted with various mixed components. (a) Si2p, (b) C1s, (c) O1s, and (d) N1s.

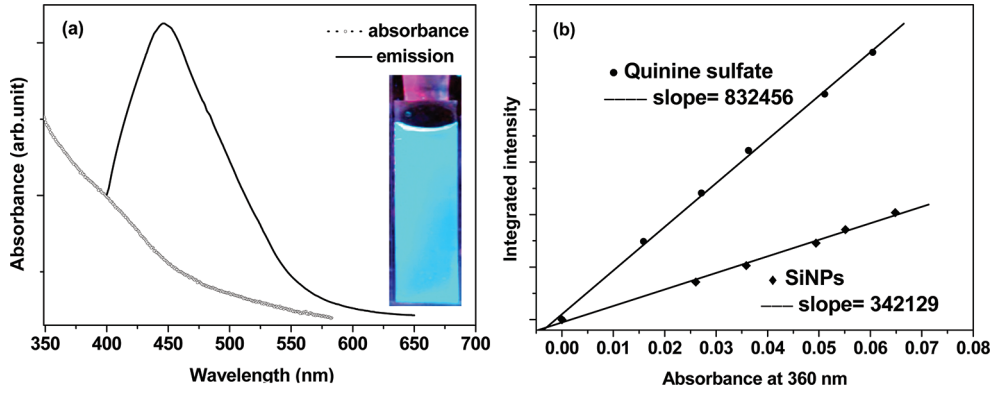

Figure 5. (a) Dotted line shows the absorption spectrum of amine-capped SiNPs in water; the solid line shows the photoluminescence spectrum of amine-capped SiNPs in water at an excitation at 360 nm. The inset image shows the fluorescence from a vial of amine-capped SiNPs in water when excited with a UV lamp. (b) Integrated PL intensity versus absorbance for multiple diluted SiNPs in water and for various dilution of quinine sulfate in 0.5 M H_2SO_4 under identical excitation conditions.

solution of SiNPs in water with absorbances between 0.1 and 0.01 was prepared and the gradient of the plot of integrated fluorescence intensity against absorbance was found. The quantum yield of our amine-terminated SiNPs was found to be at approximately 22% with an excitation wavelength at 360 nm. The observed QY value in water is comparable to values of QY for SiNPs reported in the literature, which range from 2 to 18% in water.[10,11]

It is well-known that the amine moiety can strongly quench the emission of semiconductor quantum dots under certain pH values,[57] so it is interesting to investigate this phenomenon to determine the effect of pH upon the emission characteristics of amine-terminated SiNPs. With this aim, we obtained PL spectra from SiNPs over a range of pH environments (4−14) (see Figure S6 in the Supporting Information), and observed that the maximum emission peak position is independent of the pH.

dx.doi.org/10.1021/am300642m | ACS Appl. Mater. Interfaces 2012, 4, 3285−3292

This implies that the synthesized SiNPs remain stable in extremely acidic or in basic conditions and that the emission with protonated (nonquencher) and nonprotonated (quencher) amine groups originates from the same state. At low pH the amine group is protonated, and electron transfer between the amine moieties and the Si core is prohibited, yielding higher emission intensity.[32] At higher pH, protonation is either incomplete or absent, which allows involvement of the nitrogen lone pair in relaxation processes and yields a reduced emission.[32]

Table 1. Quantum Yields of Amine-Capped SiNPs in Water Solutions of Different pH Values and PBS Expressed As the Percentage of Photons Emitted Per Photon Absorbed, Using Quinine Sulphate As Standard Reference

solvent (pH)	quantum yield (%)
water (4)	23 ± 3
water (7)	22 ± 3
water (9)	16 ± 5
PBS (7)	18 ± 5

The lack of PL stability of nanostructured silicon is one of the major barriers to the commercial application.[10] To investigate the PL stability in PBS and water further, we measured time-dependent PL spectra of amine-terminated SiNPs by monitoring the emission using an excitation wavelength of 360 nm, see Figure 6 below and Figure S7 in the Supporting Information.

In the results shown in Figure 6 and Figure S7 in the Supporting Information, one can observe the PL from amine-capped SiNPs decays over a month, but is still strong (about two-thirds of initial PL intensity). This is a much better product than other semiconductor QDs. Although the monolayers formed on single crystal silicon surfaces are robust toward oxidation over long periods, it is likely that the monolayers on these small particles contain more defects or are less ordered and therefore water can penetrate to the underlying Si atoms. For SiNPs of 4−5 nm in diameter, red luminescence is common, although there remains some dispute concerning its origin. The blue-shifting of the emission to blue-green observed in the NPs studied here may be indicative of surface oxidation taking place, leading to a reduction in the particle size. Similar shifting has been recently reported in small NPs (<10 nm) after treatment by laser ablation was attributed to the same reason, with PL maxima shifting from 490 nm (blue) to 425 nm.[58]

Different types of nanoparticles possess their own particular physicochemical properties, which in turn determines their potential toxicity or lack thereof. Amine capping has been applied to a variety of nanoparticles in order to render them compatible with biological media.[59] The effect of amine-capped SiNPs on the proliferation of cells was determined by MTT assay. HepG2 cells were plated in 200 μL of complete culture medium containing 0.1−200 μg mL^{-1} concentrations of amine-capped SiNPs in 96-well plates for 48 h. There was no evidence of morphology change when the cells were observed under a phase-contrast microscope. The values of cytotoxicity induced by exposure to amine-capped SiNPs are given in Figure 7. As

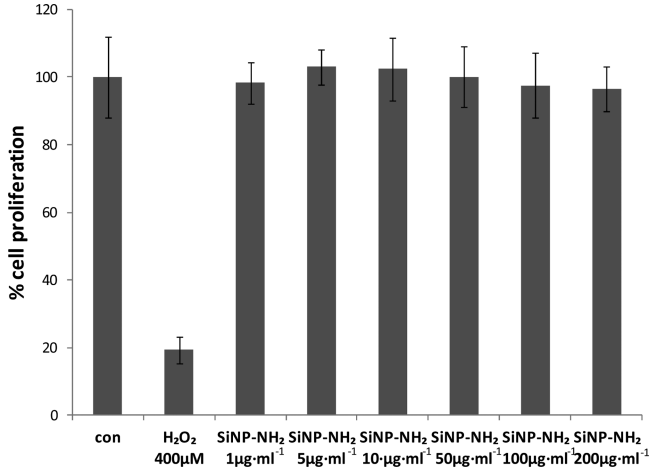

Figure 7. MTT assay of amine-capped silicon nanoparticles in HepG2 cells.

shown in Figure 7, treatment with amine functionalized nanoparticles (0−200 μg mL^{-1}) did not remarkedly affect the proliferation of HepG2 cells. Amine-capped SiNPs treatment (0−200 μg mL^{-1}) did not result in a dose-dependent inhibition of cell growth, as compared to vehicle-treated controls.

Confocal microscope images are shown in Figure 8. Nuclei were stained with DAPI are shown in Figure 8 (a). Bright fluorescence has arisen from the emission of SiNPs, see Figure 8b. The image observed in bright field and merged results are

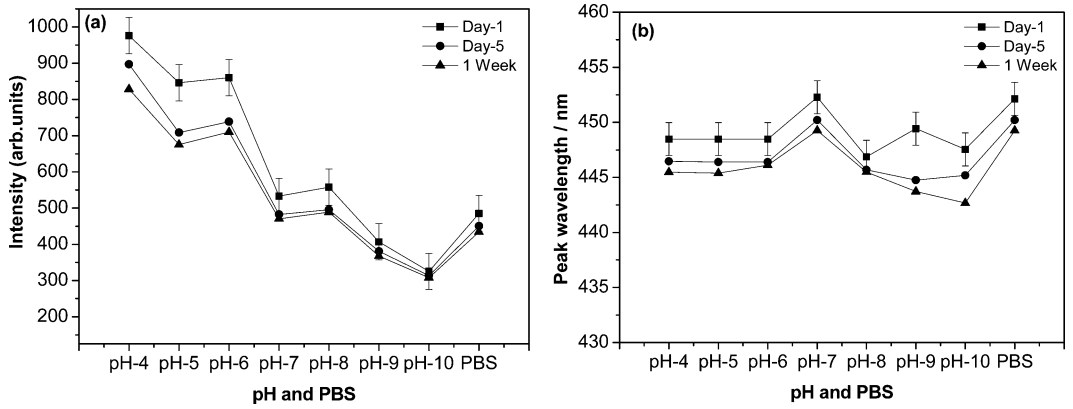

Figure 6. Aging effect on luminescence spectra for amine-capped SiNPs in water at different pH values and in PBS (excitation wavelength = 360 nm): (a) peak intensity; (b) peak wavelength. The samples were stored in glass vials in the dark under ambient conditions and no attempt was made to purge the suspensions of oxygen.

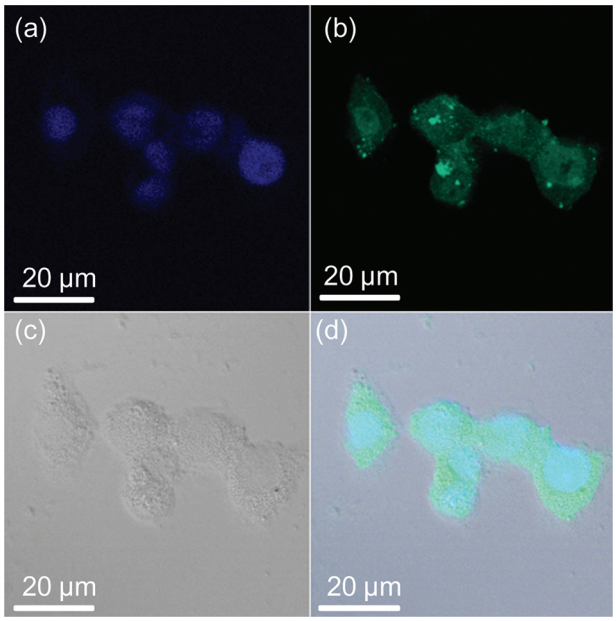

Figure 8. HepG2 cells observed under a confocal microscope, (a) nuclei staining with DAPI; (b) fluorescence from the amine-capped SiNPs; (c) bright field; and (d) combination of all three.

also shown in Figure 8c, d. The fluorescence is almost evenly distributed throughout the cells. However, higher concentrations can be observed in nuclei, where fluorescence overlaps with the DAPI stain. Importantly, no signs of morphological damage to cells is observed upon treatment with the amine-capped SiNPs in DI water. Such a result is in contrast to recent studies, which suggest the positive charge of the amine-terminated surface can lead to an increase in cytotoxicity.[60] This is a significant advance in the biological applications of SiNPs. Otherwise, choosing a suitable solvent would be critical.[18,61]

4. CONCLUSIONS

In conclusion, a facile method has been demonstrated to synthesize highly stable amine-terminated silicon nanoparticle by using electrochemically etched porous silicon. The surface of silicon quantum dots was effectively modified by using allylamine which rendered the silicon surface hydrophilicity. The obtained nanoparticles have a narrow size distribution and a very high mobility in water exposed by high-resolution TEM images and DLS and show strong blue photoluminescence under UV excitation with a luminescent quantum yield of 22%. These surface functionalized nanoparticles have remarkable photostability against degradation; they are stable for several weeks and demonstrate a great chemical stability over a wide pH range (4−14). The FTIR, NMR and XPS displayed the surface chemistry and confirmed that the surface is effectively modified with amine group. MTT assays show that amine-capped SiNPs are nontoxic to HepG2 cells.

■ ASSOCIATED CONTENT

Ⓢ Supporting Information

HRTEM images; quantum yield measurement details; stability over the pH range and time; FTIR spectrum of amine-capped Si-NPs in chloroform; and ^{1}H NMR in $CDCl_3$. This material is available free of charge via the Internet at http://pubs.acs.org.

■ AUTHOR INFORMATION

Corresponding Author

*E-mail: y.chao@uea.ac.uk.

Author Contributions

The manuscript was written through contributions of all authors. All authors have given approval to the final version of the manuscript.

Notes

The authors declare no competing financial interest.

■ ACKNOWLEDGMENTS

J.A. is thankful for a Tyndall studentship and an ORS award. This research is supported by EPSRC under Grant EP/G01664X/1. NCESS is acknowledged for awarding XPS beamtime and the help of Dr. Danny Law is gratefully received. LENNF is thanked for HRTEM access.

■ REFERENCES

(1) Nirmal, M.; Brus, L. *Acc. Chem. Res.* **1999**, *32*, 407−414.
(2) Zhu, X.; Yukawa, T.; Kishi, T.; Hirai, M.; Suematsu, H.; Jiang, W.; Yatsui, K. *J. Nanopart. Res.* **2005**, *7*, 669−673.
(3) Chao, Y.; Šiller, L.; Krishnamurthy, S.; Coxon, P. R.; Bangert, U.; Gass, M.; Kjeldgaard, L.; Patoleo, S. N.; Lie, L. H.; O'Farrell, N.; Alsop, T. A.; Houlton, A.; Horrocks, B. R. *Nat. Nanotechnol.* **2007**, *2*, 486−489.
(4) Froner, E.; Adamo, R.; Gaburro, Z.; Margesin, B.; Pavesi, L.; Rigo, A.; Scarpa, M. *J. Nanopart. Res.* **2006**, *8*, 1071−1074.
(5) Belomoin, G.; Therrien, J.; Smith, A.; Rao, S.; Twesten, R.; Chaieb, S.; Nayfeh, M. H.; Wagner, L.; Mitas, L. *Appl. Phys. Lett.* **2002**, *80*, 841−843.
(6) English, D. S.; Pell, L. E.; Yu, Z.; Barbara, P. F.; Korgel, B. A. *Nano Lett.* **2002**, *2*, 681−685.
(7) Schuppler, S.; Friedman, S. L.; Marcus, M. A.; Adler, D. L.; Xie, Y. H.; Ross, F. M.; Chabal, Y. J.; Harris, T. D.; Brus, L. E.; Brown, W. L.; Chaban, E. E.; Szajowski, P. F.; Christman, S. B.; Citrin, P. H. *Phys. Rev. B* **1995**, *52*, 4910.
(8) Rogozhina, E.; Belomoin, G.; Smith, A.; Abuhassan, L.; Barry, N.; Akcakir, O.; Braun, P. V.; Nayfeh, M. H. *Appl. Phys. Lett.* **2001**, *78*, 3711−3713.
(9) Rosso-Vasic, M.; Spruijt, E.; van Lagen, B.; De Cola, L.; Zuilhof, H. *Small* **2008**, *4*, 1835−1841.
(10) Warner, J. H.; Hoshino, A.; Yamamoto, K.; Tilley, R. D. *Angew. Chem., Int. Ed.* **2005**, *44*, 4550−4554.
(11) Erogbogbo, F.; Yong, K.-T.; Roy, I.; Xu, G.; Prasad, P. N.; Swihart, M. T. *ACS Nano* **2008**, *2*, 873−878.
(12) Mayne, A. H.; Bayliss, S. C.; Barr, P.; Tobin, M.; Buckberry, L. D. *Phys. Status solidi A* **2000**, *182*, 505−513.
(13) Kirchner, C.; Liedl, T.; Kudera, S.; Pellegrino, T.; Muñoz Javier, A.; Gaub, H. E.; St√∂lzle, S.; Fertig, N.; Parak, W. J. *Nano Lett.* **2004**, *5*, 331−338.
(14) Nilsson, J. R. *Acta Protozool* **2003**, *42*, 19−29.
(15) Pelley, J. L.; Daar, A. S.; Saner, M. A. *Toxicol. Sci.* **2009**, *112*, 276−296.
(16) Arya, H.; Kaul, Z.; Wadhwa, R.; Taira, K.; Hirano, T.; Kaul, S. C. *Biochem. Biophys. Res. Commun.* **2005**, *329*, 1173−1177.
(17) Miller, D. A. B. *Nature* **1995**, *378*, 238.
(18) Alsharif, N. H.; Berger, C. E. M.; Varanasi, S. S.; Chao, Y.; Horrocks, B. R.; Datta, H. K. *Small* **2009**, *5*, 221−228.
(19) Buriak, J. M. *Chem. Commun.* **1999**, 1051.
(20) Tilley, R. D.; Yamamoto, K. *Adv. Mater.* **2006**, *18*, 2053−2056.
(21) Neiner, D.; Chiu, H. W.; Kauzlarich, S. M. *J. Am. Chem. Soc.* **2006**, *128*, 11016−11017.
(22) Zhang, X.; Neiner, D.; Wang, S.; Louie, A. Y.; Kauzlarich, S. M. *Nanotechnology* **2007**, 18.
(23) Yu, Z. R.; Aceves-Mijares, M.; Cabrera, M. A. I. *Nanotechnology* **2006**, *17*, 3962−3967.

(24) Chao, Y.; Krishnamurthy, S.; Montalti, M.; Šiller, L.; Lie, L. H.; Houlton, A.; Horrocks, B. R.; Kjeldgaard, L.; Dhanak, V. R.; Hunt, M. R. C. *J. Appl. Phys.* **2005**, *98*, 044316.
(25) Lie, L. H.; Duerdin, M.; Tuite, E. M.; Houlton, A.; Horrocks, B. R. *J. Electroanal. Chem.* **2002**, *538*−*539*, 183−190.
(26) Hua, F.; Erogbogbo, F.; Swihart, M. T.; Ruckenstein, E. *Langmuir* **2006**, *22*, 4363−4370.
(27) Hua, F. J.; Swihart, M. T.; Ruckenstein, E. *Langmuir* **2005**, *21*, 6054−6062.
(28) Michalet, X.; Pinaud, F. F.; Bentolila, L. A.; Tsay, J. M.; Doose, S.; Li, J. J.; Sundaresan, G.; Wu, A. M.; Gambhir, S. S.; Weiss, S. *Science* **2005**, *307*, 538−544.
(29) Zhou, Z.; Brus, L.; Friesner, R. *Nano Lett.* **2003**, *3*, 163−167.
(30) Canham, L. T. *Appl. Phys. Lett.* **1990**, *57*, 1046−1048.
(31) Bisero, D.; Corni, F.; Nobili, C.; Tonini, R.; Ottaviani, G.; Mazzoleni, C.; Pavesi, L. *Appl. Phys. Lett.* **1995**, *67*, 3447−3449.
(32) Rosso-Vasic, M.; Spruijt, E.; Popovic, Z.; Overgaag, K.; van Lagen, B.; Grandidier, B.; Vanmaekelbergh, D.; Dominguez-Gutierrez, D.; De Cola, L.; Zuilhof, H. *J. Mater. Chem.* **2009**, *19*, 5926−5933.
(33) Rosso-Vasic, M.; De Cola, L.; Zuilhof, H. *J. Phys. Chem. C* **2009**, *113*, 2235−2240.
(34) Tilley, R. D.; Warner, J. H.; Yamamoto, K.; Matsui, I.; Fujimori, H. *Chem. Commun.* **2005**, 1833−1835.
(35) Carter, R. S.; Harley, S. J.; Power, P. P.; Augustine, M. P. *Chem. Mater.* **2005**, *17*, 2932−2939.
(36) Giuliani, J. R.; Harley, S. J.; Carter, R. S.; Power, P. P.; Augustine, M. P. *Solid State Nucl. Magn. Reson.* **2007**, *32*, 1−10.
(37) Azzazy, H. M. E.; Mansour, M. M. H.; Kazmierczak, S. C. *Clin. Biochem.* **2007**, *40*, 917−927.
(38) Connor, E. E.; Mwamuka, J.; Gole, A.; Murphy, C. J.; Wyatt, M. D. *Small* **2005**, *1*, 325−327.
(39) Magrez, A.; Kasas, S.; Salicio, V.; Pasquier, N.; Seo, J. W.; Celio, M.; Catsicas, S.; Schwaller, B.; Forro, L. *Nano Lett.* **2006**, *6*, 1121−1125.
(40) Monteiro-Riviere, N. A.; Inman, A. O. *Carbon* **2006**, *44*, 1070−1078.
(41) Sayes, C. M.; Fortner, J. D.; Guo, W.; Lyon, D.; Boyd, A. M.; Ausman, K. D.; Tao, Y. J.; Sitharaman, B.; Wilson, L. J.; Hughes, J. B.; West, J. L.; Colvin, V. L. *Nano Lett.* **2004**, *4*, 1881−1887.
(42) Shukla, R.; Bansal, V.; Chaudhary, M.; Basu, A.; Bhonde, R. R.; Sastry, M. *Langmuir* **2005**, *21*, 10644−10654.
(43) Mosmann, T. *J. Immunol. Methods* **1983**, *65*, 55−63.
(44) Wang, Q.; Bao, Y.; Zhang, X.; Coxon, P. R.; Jayasooriya, U. A.; Chao, Y. *Adv. Health. Mater.* **2012**, *1*, 189−198.
(45) Wang, J.; Sun, S.; Peng, F.; Cao, L.; Sun, L. *Chem. Commun.* **2011**, *47*, 4941−4943.
(46) Shiohara, A.; Hanada, S.; Prabakar, S.; Fujioka, K.; Lim, T. H.; Yamamoto, K.; Northcote, P. T.; Tilley, R. D. *J. Am. Chem. Soc.* **2009**, *132*, 248−253.
(47) Chao, Y.; Wang, Q.; Pietzsch, A.; Hennies, F.; Ni, H. *Phys. Status Solidi A* **2011**, *208*, 2424−2429.
(48) Wang, Q.; Ni, H.; Pietzsch, A.; Hennies, F.; Bao, Y.; Chao, Y. *J. Nanopart. Res.* **2011**, *13*, 405−413.
(49) *X-ray Data Booklet*; Lawrence Berkeley National Laboratory: Berkeley, CA, 2001.
(50) Wagner, C.; Riggs, W.; Davis, L.; Moulder, J. In *Handbook of X-ray Photoelectron Spectroscopy*; Muilenberg, G. E., Ed.; Perkin Elmer Corporation: Eden Prairie, MN, 1997.
(51) Dementjev, A. P.; de Graaf, A.; van de Sanden, M. C. M.; Maslakov, K. I.; Naumkin, A. V.; Serov, A. A. *Diamond Relat. Mater.* **2000**, *9*, 1904−1907.
(52) Coxon, P. R.; Wang, Q.; Chao, Y. *J. Phys. D: Appl. Phys.* **2011**, *44*, 495301.
(53) Wolkin, M. V.; Jorne, J.; Fauchet, P. M.; Allan, G.; Delerue, C. *Phys. Rev. Lett.* **1999**, *82*, 197−200.
(54) Šiller, L.; Krishnamurthy, S.; Kjeldgaard, L.; Horrocks, B. R.; Chao, Y.; Houlton, A.; Chakraborty, A. K.; Hunt, M. R. C. *J. Phys.-Condens. Matter* **2009**, *21*, 095005.
(55) Sato, S.; Swihart, M. T. *Chem. Mater.* **2006**, *18*, 4083−4088.
(56) Xiong, H. M.; Wang, Z. D.; Xia, Y. Y. *Adv. Mater.* **2006**, *18*, 748−751.
(57) Landes, C. F.; Braun, M.; El-Sayed, M. A. *J. Phys. Chem. B* **2001**, *105*, 10554−10558.
(58) Alkis, S.; Okyay, A. K.; Ortac, B. *J. Phys. Chem. C* **2012**, *116*, 3432−3436.
(59) Lee, S. H.; Bae, K. H.; Kim, S. H.; Lee, K. R.; Park, T. G. *Int. J. Pharm.* **2008**, *364*, 94−101.
(60) Bhattacharjee, S.; de Haan, L. H. J.; Evers, N. M.; Jiang, X.; Marcelis, A. T. M.; Zuilhof, H.; Rietjens, I. M. C. M.; Alink, G. M. *Particle Fibre Toxicol.* **2010**, 7.
(61) Dickinson, F. M.; Alsop, T. A.; Al-Sharif, N.; Berger, C. E. M.; Datta, H. K.; Siller, L.; Chao, Y.; Tuite, E. M.; Houlton, A.; Horrocks, B. R. *Analyst* **2008**, *133*, 1573−1580.